

1 Spectrometric measurements of atmospheric propane (C₃H₈)

2 Geoffrey C. Toon¹, Jean-Francois L. Blavier¹, Keeyoon Sung¹, Katelyn Yu^{1,2}

3 ¹ Jet Propulsion Laboratory, California Institute of Technology, Pasadena, CA, 91109, USA

4 ² Dept. Civil and Environmental Engineering, UC Berkeley, Berkeley, CA, 94720, USA

5 Correspondence to: Geoffrey.C.Toon@jpl.nasa.gov

6 **Abstract.** We report measurements of atmospheric C₃H₈ from analysis of ground-based, solar absorption spectra
7 from the JPL MkIV interferometer. Using the strong Q-branch absorption feature at 2967 cm⁻¹, we can measure
8 C₃H₈ in locations where its abundance is enhanced by proximity to sources (e.g., large natural gas fields, mega-
9 cities). A case study of MkIV C₃H₈ measurements from Ft. Sumner, New Mexico, shows that amounts are strongly
10 correlated with ethane (C₂H₆) and with back-trajectories from SE New Mexico and West Texas, where the Permian
11 Basin oil and natural gas field is located. Measurements from JPL, California, also show large C₃H₈ enhancements
12 on certain days, but more correlated with CO than C₂H₆. ~~From high-altitude, balloon-borne, MkIV solar occultation~~
13 ~~measurements, C₃H₈ was not detected at any altitude (5-40 km) in any of its 25 flights.~~

14 1. Introduction

15 Non-methane hydrocarbons such as C₃H₈ and C₂H₆ affect air quality because their oxidation enhances tropospheric
16 O₃ and aerosol pollution. They are also sensitive indicators of fugitive losses by the oil and natural gas industry, an
17 important source of co-emitted methane (CH₄), a greenhouse gas. These fugitive losses appear to be under-
18 estimated in global inventories (Dalsoren et al., 2018).

19 Atmospheric C₃H₈ and C₂H₆ are entirely the result of emissions at the surface. In pre-industrial times these came
20 from geological seeps and wild fires, but in recent times these natural sources have been surpassed by emissions
21 from fossil fuel production. The latter peaked in about 1970, and then declined due to stricter regulation of
22 emissions from the oil and natural gas industry and automobiles. But in the past decade, this decreasing trend has
23 reversed due to accelerated Natural Gas (NG) exploitation (Helmig et al., 2016).

24 C₃H₈ has a lifetime of about 2 weeks in summer and 8 weeks in winter (Rosado-Reyes et al., 2007). This is mostly
25 dictated by how fast it is being oxidized by reactions with hydroxyl radicals and chlorine atoms. Given this 2–8
26 week lifetime, a single strong source of propane has the potential to degrade air quality over most of the hemisphere.

27 Unprocessed, in-the-ground, “wet” natural gas is usually between 70–95% CH₄, 1–15% C₂H₆, 1–10% C₃H₈, and 0–
28 3% C₄H₁₀. The latter two gases are typically extracted to form Liquefied Petroleum Gas (LPG). In the northern
29 hemisphere winter, LPG contains more C₃H₈, while in summer it contains more butane (C₄H₁₀), reducing variations
30 in its vapor pressure.

Deleted: large variations

Deleted: amounts

Formatted: Font: Times New Roman, 10 pt

Deleted: From MkIV solar occultation measurements from balloon, C₃H₈ was not detected at any altitude in any flight

Formatted: Font: Times New Roman, 10 pt, Subscript

Formatted: Font: Times New Roman, 10 pt

Formatted: Font: Times New Roman, 10 pt

Formatted: Font: Times New Roman, 10 pt, Subscript

Formatted: Font: Times New Roman, 10 pt

Moved down [1]: In contrast, the lifetime of C₂H₆ is 2–6 months, which is 3–4 times longer than that of C₃H₈.

Moved (insertion) [1]

Deleted: In contrast, the lifetime of C₂H₆ is 2–6 months, which is 3–4 times longer than that of C₃H₈.

39 LPG burns much more cleanly than fuel oil and is therefore increasingly used for heating, and cooking, especially in
40 rural areas that are not served by piped NG. LPG is also used to fuel commercial vehicles, and is increasingly
41 replacing CFCs as a refrigerant and as an aerosol propellant. As a result of extracting LPG from natural gas, the NG
42 that is piped to our homes in urban areas is highly depleted in C₃H₈ and C₄H₁₀, as compared with wet NG.

Deleted: is

43 To the best of our knowledge, there are no previous remote sensing measurements of C₃H₈, although in situ
44 measurements exist. Dalsoren et al. (2018, Fig.3b) show surface in situ C₃H₈ amounts below 50 ppt at Zeppelin
45 station in Svalbad in summer 2011, but with values of 1 ppb in the winter, with peaks of up to 2.4 ppb. These C₃H₈
46 peaks are strongly correlated with C₂H₆ which reaches 3.4 ppb. Using in situ C₃H₈ data from multiple sites Helmig et
47 al. (2016) show a large seasonal cycle in surface in situ C₃H₈ at high NH latitudes, reaching 1 ppb in winter, with
48 little in the SH. They also show increasing C₃H₈ over central and Eastern US over the period 2009.5–2014.5, but no
49 increase on the West coast.

Deleted: report

Deleted: of essentially zero

Deleted: a

50 Since C₃H₈ correlates with C₂H₆, both having NG as their main source, we also consider the previous measurements
51 of C₂H₆, which has a lifetime of 2-8 months, 4 times longer than propane. Angelbratt et al. (2011) reported a 0–
52 2%/year decline over the period 1996 to 2006 based on data from six NH FTIR sites. Franco et al (2015) reported a
53 shallow minimum in C₂H₆ in the 2005–2010 period based on ground-based FTIR solar spectra above the
54 Jungfraujoch scientific station. Helmig et al. (2016) report a minimum in atmospheric C₂H₆ in 2005–2010 based on
55 in situ and remote measurements.

Deleted: .

56 Franco et al. (2016) estimate a 75% increase in North American C₂H₆ emissions between 2008 and 2014, and as a
57 result report a 3–5% annual increase in column C₂H₆ at Northern mid latitudes. They hypothesize that this increase
58 is the result of the recent massive growth in the exploitation of shale gas and tight oil reservoirs in North America,
59 where the drilling productivity began to grow rapidly after 2009.

60 2. Methods

61 2.1 MkIV Instrument

62 The JPL MkIV interferometer (Toon, 1991) is a high-resolution FITR spectrometer built at JPL in 1984. It covers
63 the entire 650–5650 cm⁻¹ range simultaneously in every spectrum with two detectors: a HgCdTe photoconductor
64 covering 650–1800 cm⁻¹ and an InSb photodiode covering 1800–5650 cm⁻¹. For ground-based observations a
65 maximum OPD of 117 cm is employed providing a spectral resolution of 0.005 cm⁻¹. The MkIV is primarily a
66 balloon instrument and has performed 25 flights since 1989, the latest in 2019. Between balloon flights it makes
67 ground-based observations. Since 1985 it has taken 5000 ground-based observations on 1200 different days from 12
68 different sites. For more detail, see tables in: <https://mark4sun.jpl.nasa.gov/ground.html>

Deleted: K

Deleted: K

69 2.2 Retrieval

77 The analysis of the MkIV spectra was performed with the GFIT (Gas Fitting) tool, a nonlinear, least-squares,
78 spectral-fitting, algorithm developed at JPL. GFIT has been previously used for the Version 3 analysis (Irion et al.,
79 2002) of spectra measured by the Atmospheric Trace Molecule Occultation Spectrometer, and it is currently used for
80 analysis of Total Carbon Column Observing Network (TCCON) spectra (Wunch et al., 2011) and for MkIV spectra
81 (Toon et al., 2016; 2018a; 2018b). The entire package including spectral fitting software, spectroscopic linelists, and
82 software to generate a priori VMR/T/P profiles, is termed GGG.

83 GFIT scales the atmospheric gas volume mixing ratio (VMR) profiles to fit calculated spectra to those measured.
84 For C₃H₈, a 5.4 cm⁻¹-wide fitting window centered on the Q-branch at 2967 cm⁻¹ was used. The atmosphere was
85 discretized into 70 layers of 1 km thickness. C₃H₈ and four interfering gases (H₂O, CH₄, C₂H₆, HDO) were adjusted.
86 Two frequency stretches were retrieved (telluric and solar). The spectral continuum was fitted as a straight line, and
87 a zero-level offset was fitted. So that's a total of 10 simultaneously-fitted scalars. In addition, the solar pseudo-
88 transmittance was computed (but not adjusted).

89 The assumed temperature, pressure and H₂O profiles were based on the NCEP 6-hourly analyses for solar noon of
90 each day. The a priori vmr profiles were based on NH mid-latitude profiles. This is the same scheme as used by the
91 GGG TCCON analysis (Wunch et al., 2015), but here we apply it to the Mid-IR MkIV spectra rather than the Short-
92 Wave IR TCCON spectra.

93 To estimate the sensitivity of the retrieved C₃H₈ to uncertainties in the assumed a priori profiles of T/P and
94 interfering gases (especially H₂O, CH₄), we retrieve the post-2000 C₃H₈ a second time: using GGG2020, an updated
95 version of the GGG code with improved a priori VMR/T/P profiles based on the GEOS-FP-IT analysis (Laughner et
96 al., 2021). The results, shown in figure B.2, illustrate that this changes the retrieved C₃H₈ by less than 10% with a
97 bias of only 1.1%.

98 2.3. Spectroscopy

99 It is clear from the infra-red lab spectrum of C₃H₈ (Fig.1), measured at Pacific North-West National Laboratory
100 (Sharpe et al., 2004), that the feature at 2967 cm⁻¹, caused by various CH₂ and CH₃ stretch vibrational modes, is by
101 far the strongest in the entire infrared. So for solar occultation spectrometry, this is by far the best choice. For
102 thermal emission spectrometry from cold planets such as Titan, however, these bands are not covered by
103 Cassini/CIRS since the thermal Plank function of such planets weakens rapidly above 2000 cm⁻¹. Thus, the much
104 weaker bands below 1400 cm⁻¹ must be used (Sung et al., 2013).

Deleted: K

Deleted: 3

Deleted: exactly

Deleted: 2014

Deleted: W

Deleted: instead of GGG2014

Deleted: appendix

Deleted: A

Deleted: show

Deleted: rms

Deleted: lab

Formatted: Font color: Text 1

Formatted: Font: Times New Roman, 10 pt, Not Italic, Font color: Text 1

Formatted: Font color: Text 1

Formatted: Font: Times New Roman, 10 pt, Not Italic, Font color: Text 1

Deleted: . For thermal emission spectrometry from cold planets such as Titan, on the other hand, then the much weaker CH₃ deform bands around 1400 cm⁻¹ would be better (Sung et al., 2013).

Formatted: Font: 10 pt

Formatted: Superscript

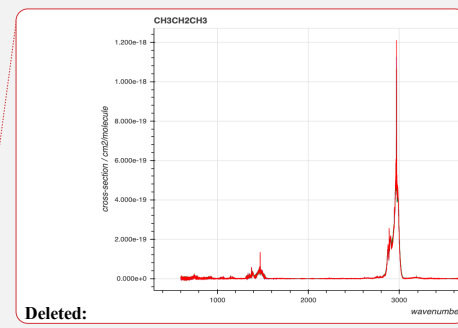
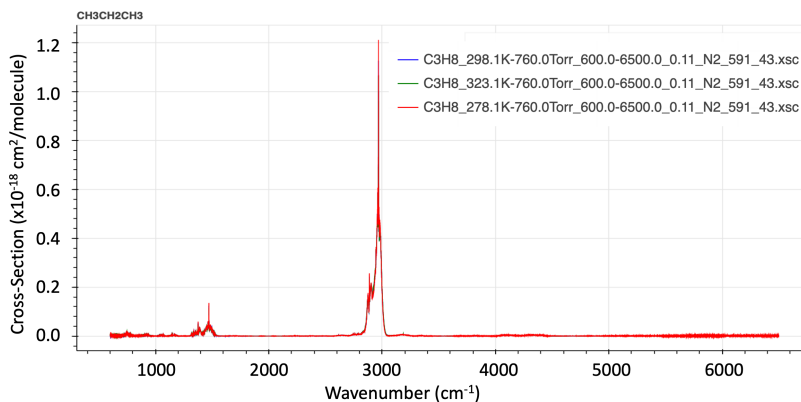
Formatted: Font: 10 pt

Formatted: Font: 10 pt, Superscript

Formatted: Font: 10 pt

Formatted: Font: 10 pt

Formatted: Font: 10 pt



Deleted: laboratory
Formatted: Font: Italic

120

121 **Figure 1.** Infrared spectra of PNNL C₃H₈ absorption cross-section at 323, 298, and 278K (from hitran.org).

122 An empirical pseudo-line-list (EPLL) of C₃H₈ covering 2560–3280 cm⁻¹ was derived from the laboratory cross-
 123 sections of Harrison and Bernath (2010b). This is described in the unpublished report:
 124 https://mark4sun.jpl.nasa.gov/data/spec/Pseudo/c3h8_pll_2560_3280.pdf

125 The use of an EPLL facilitates interpolation and extrapolation of the lab cross-sections to T/P conditions that were
 126 not measured in the lab. The fitting of the EPLL also checks the self-consistency of the lab cross-section spectra,
 127 and provides an opportunity to correct for artifacts in the lab spectra (e.g., channeling, zero-level offsets,
 128 contamination, ILS), although it must be stated that in this particular case the C₃H₈ lab spectra were of very high
 129 quality and comprehensive in terms of their coverage. For the interfering C₂H₆, an EPLL developed eight years ago
 130 was used, based on lab measurements of Harrison et al. (2010a), as described in the report:
 131 https://mark4sun.jpl.nasa.gov/report/C2H6_spectroscopy_evaluation_2850-3050_cm-1.compressed.pdf

132 For other gases the atm.161 linelist was used, which is based on HITRAN 2016, with some empirical adjustments
 133 based on fits to lab spectra, especially for H₂O and CH₄. This is basically the same linelists (atm.161, pll.101) that
 134 are used by TCCON, but here we use them in the MIR rather than the SWIR.

135 Figure 2 shows an average spectral fit to the C₃H₈ window in ground-based MkIV spectra, obtained by fitting
 136 individual spectra and then averaging the results. The lower panel provides the full transmittance y-range from 0 to
 137 1. It can be seen that the main absorbers are CH₄ (orange) and H₂O (green). The C₃H₈ absorption (red) is difficult to
 138 discern because it is so shallow. The lower-middle panel shows the same spectral fit, but with the y-scale zoomed
 139 into 0.95–1.00 transmittance, allowing the weak absorbers like C₃H₈ and C₂H₆ to be more easily seen. The “other”
 140 contributions (e.g., O₃) were included in the calculation but not adjusted. The C₃H₈ absorption is fairly flat at about
 141 1% depth, except for the Q-branch where it deepens to 2½%. Although the strongest C₂H₆ feature coincides with the
 142 C₃H₈ Q-branch, the former is much narrower and there are several additional C₂H₆ features in this window, so the

Deleted: we expect little

182 extracted from such spectral fits. But since the analysis of the MkIV spectra is highly automated, it took only a few
 183 hours to run the C₃H₈ window over all 5000 MkIV ground-based spectra.

184

185 3. Results

186 Table 1 lists the observation sites from where MkIV has made ground-based observations up to the end of 2019. The
 187 vast majority are from three sites: JPL, Mt. Barcroft, and Ft. Sumner.

188

Town	State	N _{obs}	N _{day}	Latitude (deg.)	Longitude (deg.)	Altitude (km)	Terrain	Years Operated
Esrang	Sweden	160	32	67.889	+21.085	0.271	Boreal	1999–2007
Fairbanks	Alaska	124	46	64.830	-147.614	0.182	Boreal	1997
Lynn Lake	Manitoba	20	11	56.858	-101.066	0.354	Boreal	1996
Mt. Barcroft	California	1369	258	37.584	-118.235	3.801	Alpine	1994–2002
Mtn. View	California	7	4	37.430	-122.080	0.010	Urban	1987, 2001
Daggett	California	33	21	34.856	-116.790	0.626	Desert	1993
Ft. Sumner	New Mex.	521	106	34.480	-104.220	1.260	Steppe	1989–2019
TMF	California	475	45	34.382	-117.678	2.257	Alpine	1986–2009
JPL (B183)	California	2273	690	34.199	-118.174	0.345	Urban	1985–2020
JPL (mesa)	California	20	5	34.205	-118.171	0.460	Urban	1988–1989
Palestine	Texas	4	3	31.780	-95.700	0.100	Rural	1989
McMurdo	Antarctica	37	20	-77.847	+166.728	0.100	Polar	1986

Formatted Table

Formatted: Font color: Text 1

Formatted: Font color: Text 1

Formatted: Font color: Text 1

Formatted: Font color: Text 1

189

190 **Table 1.** The twelve sites from where MkIV has made ground-based observations, along with the number of
 191 observations and observation days from each site, years of operations, their location, and terrain type. They greved
 192 out sites have the fewest observations (only 1% of total) and are not included in the Figures 5-7 and A.1 to reduced
 193 color ambiguity.

Formatted: Font: Bold, Italic

Formatted: Font: Italic

Formatted: Font: Italic

Formatted: Font: Italic

Formatted: Font: Italic

194 Fig. 3 shows MkIV ground-based C₃H₈ columns, color coded by site altitude. The data were filtered: only points
 195 with uncertainties < 1.5x10¹⁶ were plotted, reducing the number of plotted points from 5000 to 4700. The top panel
 196 (a) shows that at the high-altitude sites (Mt. Barcroft at 3.8 km is Red; Table Mountain Facility at 2.26 km is
 197 Orange) the retrieved C₃H₈ columns are centered around zero. Also, the data acquired in Sep 1986 from 0.1 km in
 198 Antarctica (dark blue) are centered around zero. Data acquired from Ft. Sumner, NM, at 1.2 km (lime) have large
 199 variations, from zero to nearly 8x10¹⁶ molecules.cm⁻², as do the data from JPL at 0.35 km (cyan). Other sites with
 200 detectable C₃H₈ include Daggett, CA, (0.6km), Esrange, Sweden (0.26km) in the winter, Fairbanks, AK (0.2km),
 201 and Mountain View, CA in late 1991. So C₃H₈ has only been measured by MkIV from northern hemisphere sites
 202 within the PBL. Panels (b) and (c) show the same C₃H₈ columns, but plotted versus year and day.

Deleted: 5E+

Deleted: =

Deleted: =

Deleted: also

Deleted: E+

Moved (insertion) [2]

Moved up [2]: So C₃H₈ has only been measured by MkIV from northern hemisphere sites within the PBL.

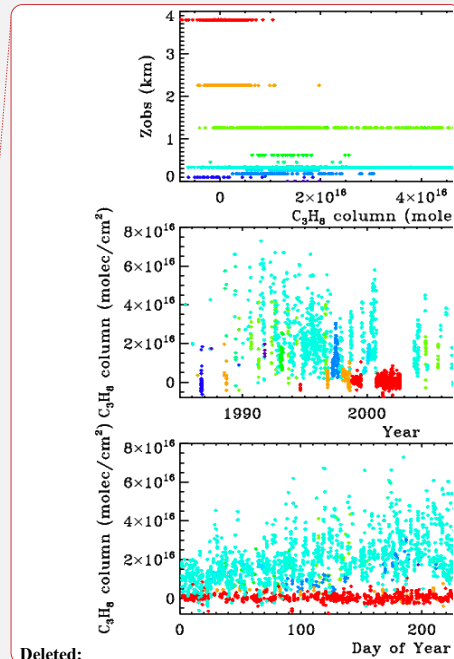
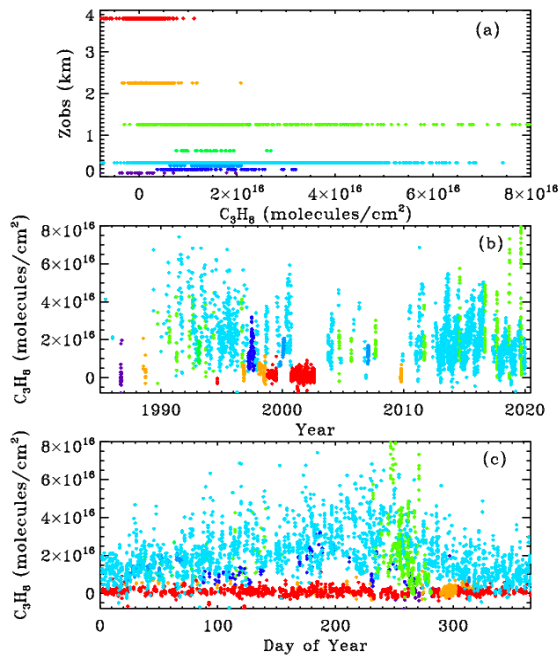
Formatted: Superscript

Deleted: , probably

Deleted: ing

203 High C₃H₈ values (>4x10¹⁶ molecules.cm⁻²) can occur at any time of year at JPL (cyan) but most commonly in late
 204 summer, as is the case for other pollutants, e.g. CO. This reflects the meteorology (stagnant conditions in the LA

214 basin in summer with little replacement of polluted air with clean air from outside). Averaging kernels for these
 215 C_3H_8 measurements are discussed and illustrated in Appendix B. Suffice it to say here that they range from 0.9 to
 216 1.4 and increase with altitude.



Deleted:

217

218 **Figure 3.** MkIV C_3H_8 column abundances from 8 out of 12 sites, color-coded by site altitude, as illustrated in panel
 219 (a): Violet=0.1 km (McMurdo); dark blue=0.18 km (Fairbanks); light blue=0.27 km (Esrange); cyan=0.35 km
 220 (JPL); Green=0.63 km (Daggett); lime=1.2 km (Ft. Sumner); orange=2.26 km (TMF); red=3.8 km (Mt. Barcroft).

- Deleted: all
- Deleted: blue
- Deleted: 0
- Deleted: 5

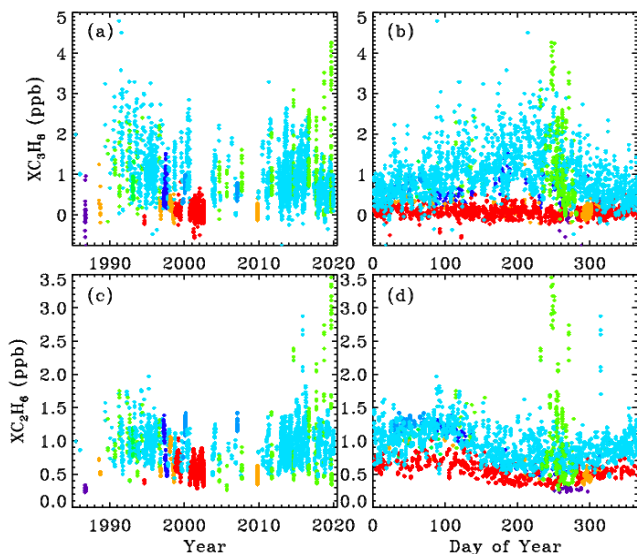
221 The reported uncertainties in our C_3H_8 column measurements are based on the rms fitting residuals compared with
 222 the sensitivity of the spectrum to C_3H_8 (Jacobians). At the highest site, Barcroft at 3.8 km ($P=0.65$ atm.), where the
 223 interfering H_2O and CH_4 absorptions are relatively weak and narrow, the C_3H_8 column uncertainties are generally
 224 smaller than 10^{15} molecules. cm^{-2} . But since the columns themselves are even smaller, no C_3H_8 is detected at
 225 Barcroft. At the lower altitude sites such as JPL and Ft. Sumner, the increased interference from H_2O and CH_4 cause
 226 the C_3H_8 column uncertainties to be much larger, generally around 5×10^{15} molecules. cm^{-2} at low airmass and
 227 worsening rapidly toward higher airmasses. But the C_3H_8 increases far more, allowing C_3H_8 to be detected at these
 228 low-altitude sites under polluted conditions, despite the poorer absolute uncertainties.

- Deleted: This
- Deleted: s
- Formatted: Subscript
- Formatted: Subscript

236 High C_3H_8 values are also seen at Ft. Sumner, NM (lime), especially in recent years. This was initially a surprise to
 237 us because this area has a very low population density, so we naively assumed that we would be measuring
 238 background levels of atmospheric pollutants here.

239 We know that the apparent variations in C_3H_8 are real, rather than artifacts, from their strong correlation with C_2H_6 .
 240 Figure 4 compares column-averaged C_3H_8 mole fractions (top panels) with those of C_2H_6 (bottom panels), the latter
 241 retrieved using different spectral lines than those shown in Fig.2. These are the same total C_3H_8 columns shown in
 242 Fig.3, but divided by the total column of all gases, which is inferred from the surface pressure. The resulting
 243 column-average mole fractions, denoted X_{gas} , are less sensitive to the site altitudes being different and more easily
 244 compared with in situ measurements being in units of mole fraction.

245 The upper and lower rows of Fig.4 shows the $X_{C_3H_8}$ and $X_{C_2H_6}$ time series, respectively, plotted versus year (left)
 246 and versus day of the year (right). The data were filtered such that only points with $X_{C_3H_8}$ uncertainties < 0.74 ppb
 247 and C_2H_6 uncertainties < 0.10 ppb were plotted. This reduced the total number of points from 5000 to 4700, so only
 248 the best 94% of the data are plotted. It is clear that at JPL (cyan) C_3H_8 has decreased since the 1990s, but that at Ft.
 249 Sumner (lime) it has increased over the past decade. The data from these two sites will be explored later.



250

251 **Figure 4.** Top panels show measurements of the column-averaged C_3H_8 mole fractions ($X_{C_3H_8}$). Bottom panels
 252 show $X_{C_2H_6}$. Left panels show the variation with year. Right-hand panels show the seasonal variation. Points are
 253 color-coded by observation site altitude as in Fig.3.

Deleted: c

Formatted: Font: Times New Roman, 10 pt

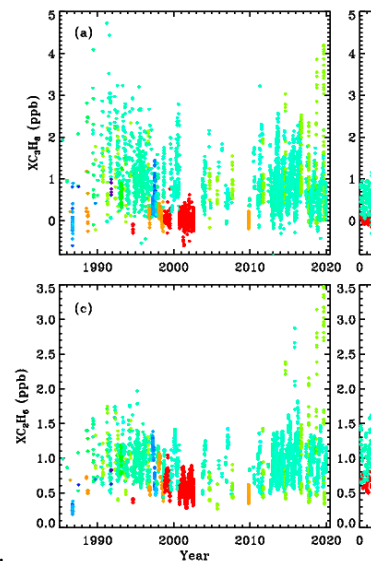
Formatted: Font: Times New Roman, 10 pt

Formatted: Font: Times New Roman, 10 pt

Formatted: Font: Times New Roman, 10 pt

Deleted: The left-hand panels of Fig.4 show the $X_{C_3H_8}$ time series plotted versus year, and the right-hand panels versus day of the year.

Moved down [3]: The points are color-coded by observation site altitude using the same color scheme as in Fig.3.



Deleted:

Moved (insertion) [3]

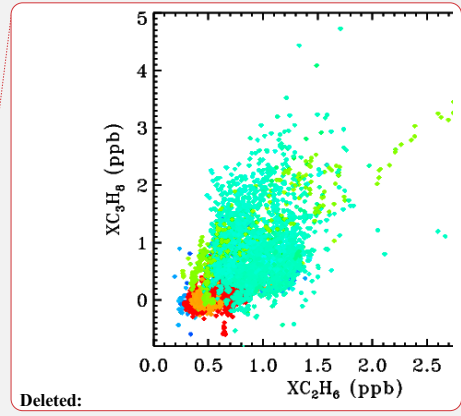
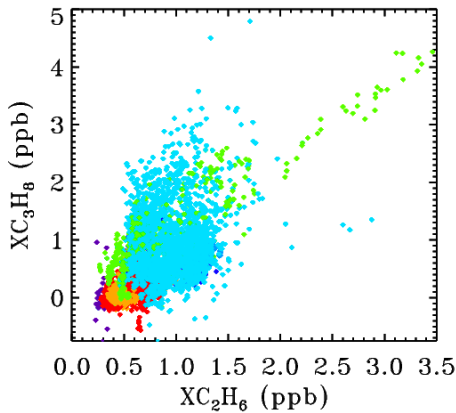
Deleted: The p

Deleted: using the same color scheme

263 C_2H_6 is four times longer-lived than C_3H_8 and never goes to zero because there is always a substantial free
 264 tropospheric C_2H_6 component, even in the SH, which varies seasonally: high in spring, low in fall. The Antarctic
 265 measurements (blue) are very low (0.2-0.3 ppb) and most probably even lower during the rest of the year, because
 266 days 250 to 300 represent the springtime peak, not the fall. The highest C_2H_6 ever measured from JPL (cyan) was in
 267 late 2015 (day 314) as a result of the Aliso Canyon natural gas leak (Conley et al., 2016). This event is further
 268 discussed later and also in Appendix C.

269 Figure 5 shows the XC_2H_6/C_3H_8 correlation plot for all sites. This uses the exact same data, filtering, and color-
 270 scheme as for Fig. 4. At JPL (cyan) the correlation is positive but weak. At Ft. Sumner, there are episodes of both
 271 gases being enhanced with a strong correlation. In fact, the highest VMRs of C_2H_6 were seen from Ft. Sumner, even
 272 more than from JPL during the Aliso Canyon gas leak in late 2015.

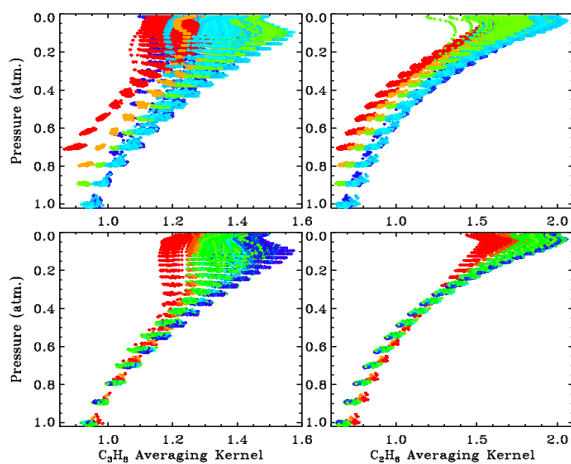
- Deleted: The lower panels of Fig.4 show XC_2H_6 . Th
- Deleted: is
- Formatted: Subscript
- Formatted: Subscript
- Deleted: that
- Formatted: Font: Times New Roman, 10 pt
- Deleted: The Antarctic measurement (blue) are even lower than they appear because
- Deleted: in Antarctica
- Deleted: ever
- Deleted: was
- Deleted: there



273
 274 **Figure 5.** The correlation between XC_2H_6 and XC_3H_8 for all sites, color-coded by site altitude as in Fig.3.

275 **3.1. Averaging Kernels.**

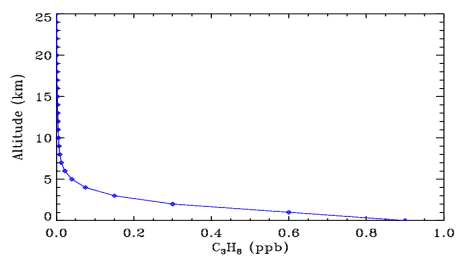
276 Figure 6 shows all kernels for the 5000 measurements presented in this paper, color-coded by site altitude (red=3.8
 277 km; orange=2.2 km; lime=1.2 km; cyan=0.35 km; blue < 0.2 km) as in the main body of the paper. The kernels
 278 increase with altitude but with <40% variation over the 0-30 km altitude range. Note that the kernels representing
 279 the 3.8 km site begin at P=0.7 atm. And the kernels representing the 2.2 km site begin at P=0.8 atm.



290

291 *Figure 6: 5000 averaging kernels for Left: C_3H_8 and Right: C_2H_6 . Upper panel shows all kernels color-coded by*
 292 *site altitude, as in Fig.3. Lower panel shows kernels for the low-altitude sites (0.25 to 0.50 km), which were all*
 293 *colored blue in the upper panel, now color-coded by solar zenith angle (Blue=15°; Green=60°; Red=80°).*

294 *The lower panel shows the kernels for the low altitude sites (mainly JPL). These points were all cyan in the upper*
 295 *panel but in the lower panel they are color-coded by Solar Zenith Angle. It is evident that the higher the SZA the*
 296 *more uniform the kernels with altitude. The banding of the points in pressure space reflects the 1 km vertical grid on*
 297 *which the kernels were computed. The C_3H_8 kernels are also influenced by the H_2O column and temperature, but*
 298 *these are smaller effects than those of site altitude or SZA.*



299

300 *Figure 7. A priori C_3H_8 profile used in these retrievals.*

301 Figure 7 show the assumed a priori vmr profile used in the retrievals and in the computation of the kernels. Since
302 GFIT performs profile scaling retrievals, with a very weak a priori constraint, the absolute values of the vmrs play
303 no role, only the profile shape matters.

Formatted: Space Before: 0 pt, After: 12 pt, Pattern: Clear

Formatted: Font: Not Bold

304 3.2. Case Study: Ground-based measurements from Ft. Sumner, NM

Deleted: 1

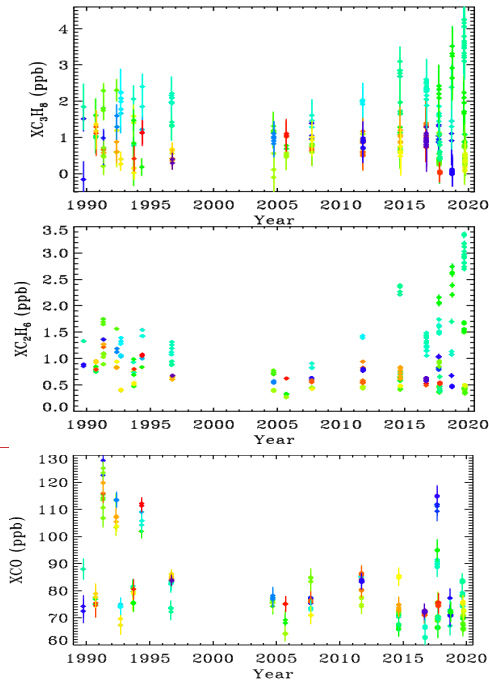
305 Ft. Sumner (34.48N, 104.22W, 1.2 km ASL) is the location of the main NASA facility for the launch of
306 stratospheric research balloons. It is located here due to the low population density and hence low risk of mishap.
307 The MkIV instrument has performed balloon campaigns in Ft. Sumner 18 times in the past 30 years. Not all of these
308 campaigns have resulted in a flight, but we have always taken ground-based observations to check that the MkIV
309 instrument is correctly aligned and functional, and to check that telemetry, commanding, and the operation of other
310 experiments do not degrade the MkIV performance.

Deleted: . A

311 We have taken 520 observations on 106 different days from Ft. Sumner (out of a total of 5000 observations and
312 1200 days). We examine these observations to try to understand whether the large day-to-day C_3H_8 variations are
313 real, and if so, what is causing them. We have already seen a correlation between the XC_3H_8 and XC_2H_6 at all sites
314 in Fig.5, but many points are buried under others, especially at the low values of XC_3H_8 and XC_2H_6 .

Formatted: Indent: First line: 0", Space Before: Auto, After: Auto

Deleted: ¶



315

316

320 **Figure 8.** XC_3H_8 , XC_2H_6 and XCO at Ft. Sumner. Since all the observations are made from the same altitude, it no
321 longer makes sense to color code by site altitude. So instead we color-code by mean bearing of the back-trajectory
322 over the previous 36 hours. Dark blue=30°; Light blue =90°; Cyan=120°; Green=180°; Lime=220°; Orange=
323 300°; Red=350°. ~~MKIV didn't visit Ft. Sumner from 1997 to 2004 because it was performing high-latitude balloon~~
324 ~~flights from Alaska and Sweden.~~

325

326 Figure 8 shows that between 1990 and 2005 there was a decrease in C_2H_6 and C_3H_8 measured in Ft. Sumner, by
327 about a factor 2 over 15 years. In recent years (since 2014), however, there has been a large increase in C_2H_6 and
328 C_3H_8 measured at Ft. Sumner, but only when the wind direction is from the SE quadrant (green-cyan colors). We see
329 no increase associated with other wind directions (red, blue, orange, yellow, lime).

330 At Ft. Sumner CO has no correlation with wind direction, nor with C_2H_6 or C_3H_8 . The majority of days have a
331 column average CO of 75 ± 10 ppb. But there are occasional enhancements up to 120 ppb, likely due to large but
332 distant fires. We do not pursue the Ft. Sumner CO data any further, beyond proving that the C_3H_8 sources are
333 different from those of CO.

334 CH_4 is also measured by MkIV. Over the 30-year measurement period XCH_4 has grown from 1650 to 1850 ppb.
335 This secular increase is much larger than any variation due to wind direction. So to be useful, the CH_4 data would
336 have to be detrended, which is not simple given its non-linear growth. Even within the past 4 years, the correlation
337 of XCH_4 with XC_3H_8 was very weak. This is to be expected since the background abundance of CH_4 is more than
338 1000x larger than C_3H_8 , whereas wet NG is only 6 times richer in CH_4 than C_3H_8 (in the Permian basin). So the NG-
339 induced enhancement of CH_4 , as a fraction of its atmospheric background level, will be much smaller than that of
340 C_3H_8 .

341 Figure 9 shows a XC_3H_8 - XC_2H_6 scatter plot using just the Ft. Sumner data. Error bars are much larger for XC_3H_8
342 than for XC_2H_6 . This is because the C_2H_6 transitions are stronger and form narrower features, both of which make
343 the retrievals more precise and definitive, whereas most of the C_3H_8 absorption is smeared into a broad continuum
344 which provides little information for retrieval in which the continuum level is fitted. The C_2H_6 features used in the
345 actual C_2H_6 retrieval are at 2976.6 and 2986.6 cm^{-1} (not shown) and are 3–4 times stronger than those seen in Fig.2.

Moved down [5]: MKIV didn't visit Ft. Sumner from 1997 to 2004 because it was performing high-latitude balloon flights from Alaska and Sweden.

Deleted: 6

Moved (insertion) [5]

Deleted: .

Deleted: 6

Deleted: /lime

Deleted: . They are of no value

Deleted: other than

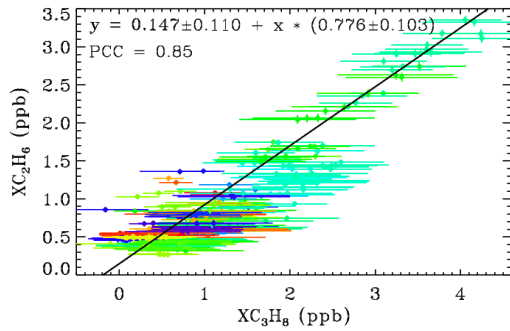
Deleted: from the Permian Basin

Deleted: .

Deleted: be more than 100 times

Deleted: 7

Deleted: this type of



360

361 **Figure 9.** The relationship between XC_3H_8 and XC_2H_6 at Ft. Sumner, color coded for wind direction as for Fig. 8.

362 The gradient of the fitted line is 0.78 ± 0.10 implying more C_3H_8 than C_2H_6 . The Pearson Correlation coefficient is
 363 0.85, which is high considering the large error bars on the XC_3H_8 , and the fact that the similarity of their Jacobians
 364 would imply an anti-correlation in their retrieved amounts (Appendix A). This tight relationship at Ft. Sumner
 365 suggests that the large variations in the C_3H_8 measurements are not an artifact. Since C_2H_6 can be easily and
 366 precisely measured by this technique, it is hard to imagine it being changed by a factor 5 from day to day by an
 367 artifact. Much more likely, the common variations in both C_3H_8 and C_2H_6 are real.

368 As already hinted, for each of the 106 observation days from Ft. Sumner we ran hourly HYSPLIT back-trajectories
 369 (Stein et al., 2015, Rolph et al., 2017) that bracket the MkIV observation times, then interpolated linearly in time
 370 between the two bracketing trajectories. This provided a unique trajectory for each of the 520 observations from Ft.
 371 Sumner. The North American Regional Reanalysis (NARR) meteorology was selected which covers North America
 372 at 32 km resolution. This is the highest resolution meteorology that covers the entire 1989–2019 observation period.
 373 A trajectory altitude of 0.4 km over Ft. Sumner was selected, and these trajectories were extended to 36 hours before
 374 the observations in 1-hour steps. Fig. 10 shows that the large variations of C_3H_8 are strongly correlated with wind
 375 direction. It is very clear that trajectories originating to the SE of Ft. Sumner, carry more C_3H_8 than those from any
 376 other direction. A plot was made also for C_2H_6 but not shown due to its strong similarity to Fig. 10.

Deleted: 7

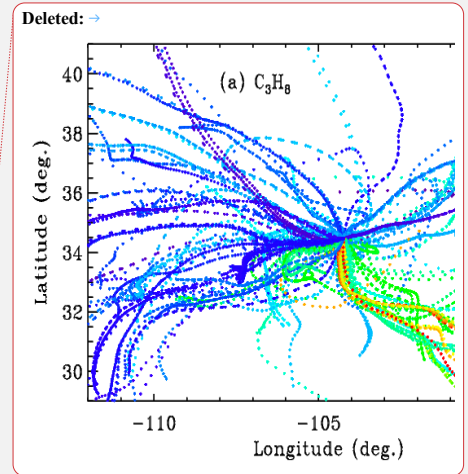
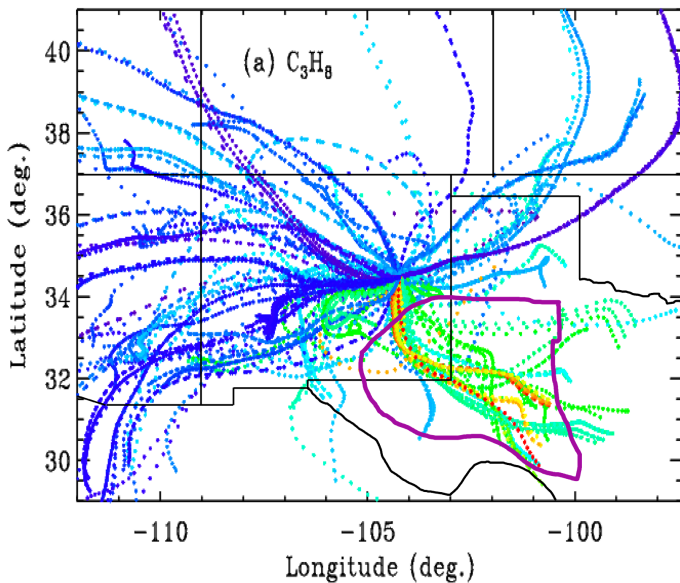
Deleted: 6

Deleted: .

Deleted: implic

Deleted: 8

Deleted: 8



383

384 **Figure 10.** Hourly locations for the back-trajectories, color-coded by retrieved XC_3H_8 . Blue=0 ppb, Green=2 ppb;
 385 Red=4 ppb. Trajectories for which the XC_3H_8 uncertainty exceeded 0.74 ppb are excluded, resulting in only 373 out
 386 of 520 trajectories being shown. Ft. Sumner lies at 34.2N, 104.2W, close to the center of the figure at the confluence
 387 of all the back-trajectories. Each point represents a 1-hour time step, so that the wind speed is apparent from the
 388 separation of points. Winds from the West are typically stronger than those from the SE quadrant. Trajectories are
 389 underlaid by a map of New Mexico and neighboring states. The Permian Basin, encircled by the thick purple line,
 390 underlies SE New Mexico and much of West Texas. Many of the trajectories from the SE have spent 30+ hours over
 391 the Permian Basin.

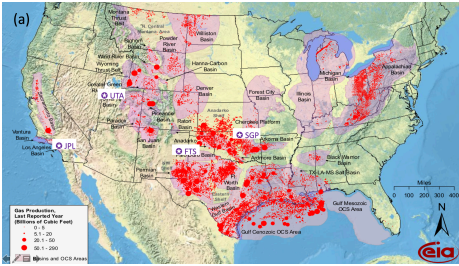
392 We also made a scatter plot for CO (not shown) but there was no correlation between CO and wind direction, or
 393 between CO and C_3H_8 . This rules out the possibility that the enhanced C_3H_8 and C_2H_6 were somehow associated
 394 with distant urban pollution or wild fires.

395 This result leads to speculation on what might be enhancing C_2H_6 and C_3H_8 when the winds come from the SE
 396 sector. One of the biggest natural gas production fields in the US lies in the Permian Basin, which underlies the
 397 South-East corner of New Mexico and West Texas, as illustrated in Figure 10. This region also includes processing
 398 plants where the heavier gases are stripped out of the wet NG, storage facilities for the resulting Natural Gas Liquids
 399 (LPG+ethane+pentane), and pipelines. The Permian Basin is by far the largest "liquids-rich" (rich in heavy
 400 hydrocarbons) gas field in the USA (https://www.spglobal.com/platts/plattscontent/_assets/_images/latest-

Deleted: 8
 Deleted: .
 Deleted:
 Deleted: nd

Deleted: 9

408 [news/20191219-rig-count.jpg](#)). This would suggest that the enhanced C₂H₆ and C₃H₈ is the result of losses from NG
 409 production, although this cannot be proven with just one instrument at one site. We would need instruments upwind
 410 and downwind to make an accurate assessment of the fluxes.



411
 412
 413 **Figure 11.** NG production in the lower 48 states of the USA in 2009. Data from the Energy Information
 414 Administration: https://www.eia.gov/oil_gas/rpd/conventional_gas.pdf. Superimposed are the locations (purple
 415 pentangular star) of the four sites discussed in detail in this paper: Ft. Sumner in Eastern NM is labelled "FTS". The
 416 JPL site in California is labelled "JPL". The locations of the NOAA sites in Utah (UTA) and Oklahoma (SGP) are
 417 also included. The Permian basin lies in the SE corner of NM and West Texas.

418 The Permian basin currently produces 16 billion cu.ft./day of NG
 419 (<https://www.eia.gov/petroleum/drilling/pdf/permian.pdf>) over an area of 220,000 km². The molar volume of an
 420 ideal gas at STP is 22.4 liters. One cu. ft. is 28.3 liters. So 16 billion cu. ft. is 20 billion moles of NG or 120x10³²
 421 molecules per day. Over an area of 220,000 km² or 2.2x10¹⁵ cm², this represents an average areal production of
 422 55x10¹⁷ molec./cm²/day. Assuming that the Permian basin is 480 km wide, at an average low-level wind speed of 15
 423 km/hour, an air parcel will take 32 hours (1.33 days) to traverse the Basin, during which time 73x10¹⁷
 424 molecules/cm² will have been extracted. Of this, 10% will be C₃H₈ (Howard et al., 2015), so if all this production
 425 were released into the atmosphere we would expect a C₃H₈ column enhancement of 73x10¹⁶.

426 In airmasses with trajectories from the SE, we see maximum C₃H₈ column enhancements of only 3x10¹⁶
 427 molecules/cm², which suggests that only 4% of the NG escapes into the atmosphere and that 96% of the NG is
 428 successfully captured (or burnt by flaring).

429 In the Permian Basin, NG is 13.7% C₂H₆ and yet the observed ethane enhancements are slightly smaller than those
 430 of C₃H₈, suggesting that only ~3% of the NG escapes. Assuming a 3% leak rate, there will also be an enhancement
 431 of CH₄ of about 14x10¹⁶ molec.cm⁻², but this represents only 0.4% of the total CH₄ column above Ft. Sumner and
 432 will therefore be difficult to discern in the presence of other confounding factors (stratospheric transport, varying
 433 tropopause altitude, seasonal and longer-term changes). Of course, all this analysis assumes that the Permian basin

- Deleted: 9
- Deleted: (a)
- Deleted: ¶
- (b): [Temporarily removed -- awaiting permission] Illustrating the high number of "liquids-rich" drilling rigs in the Permian Basin, as of Dec. 2019, underscoring its dominance for propane production in the USA. From <https://www.spglobal.com/platts/en/market-insights/latest-news/natural-gas/121919-us-oil-gas-rig-count-rises-for-second-straight-week-everus>
- Formatted: Font: Times New Roman, 10 pt
- Formatted: Line spacing: 1.5 lines
- Formatted: Font: Times New Roman, 10 pt
- Formatted: Font: Times New Roman, 10 pt
- Formatted: Font: 10 pt
- Deleted: In recent years, the Permian basin has been producing ~15 billion cu.ft. of natural gas (NG) per day (<https://www.eia.gov/petroleum/drilling/pdf/permian.pdf>). A back-of-the-envelope estimate of the contribution of this to the observed C₃H₈ is now performed. We assume that this NG production is distributed over an area that is 160 km across. At a wind speed of 20 km/hour, an airmass will take 8 hours to traverse the gas field, during which time 0.72E+19 molecules.cm⁻² of NG will have been extracted. Howard et al., (2015), measured the composition of NG from the Permian basin and found that it is very rich in heavy hydrocarbons, being 66.6% CH₄, 13.7% C₂H₆ and 10.3% C₃H₈ by volume. If 4% of this were lost to the atmosphere, and 10.3% of this is C₃H₈, the total propane column will be enhanced by 3E+16 molecules.cm⁻², which is close to that seen in the highest cases. For
- Deleted: C₂H₆,
- Formatted: Subscript
- Formatted: Subscript
- Deleted: an
- Deleted: of 4E+16
- Deleted:
- Deleted: would be expected for such a back-trajectory, which is somewhat higher than measured
- Deleted: T
- Deleted: 9E+
- Deleted: 5

469 is a uniform emitter and that the back trajectory wind speeds are accurate. There are likely hot spots with higher-
470 than-average emissions, and regions with little NG production.

471 A puzzle in our findings is that when both C₃H₈ and C₂H₆ are elevated, we measure 22% more C₃H₈ than C₂H₆ (see
472 fig.9). Yet independent essays of well-head wet NG find 33% more C₂H₆ than C₃H₈ in the Permian basin (Howard et
473 al., 2015). So we have a 55% discrepancy. We note that the C₂H₆ averaging kernel is 0.7 at the surface versus 0.9 for
474 C₃H₈ (see Appendix B). So when these gases exceed their priors in the PBL, which is likely at high enhancements,
475 both will be under-estimated, but C₂H₆ more so than C₃H₈. So this effect would cause the C₃H₈/C₂H₆ ratio to be 28%
476 high, which explains half the 55% problem. Another possibility is that the C₃H₈ coming from fugitive wet NG is
477 augmented by leaks of LPG, stripped from wet NG. This would further enhance the C₃H₈ (and C₄H₁₀) with little
478 C₂H₆ increase. Alternatively, there could be a systematic over-estimate of the MkIV C₃H₈ due to a mundane
479 multiplicative bias in the C₃H₈ spectroscopy. This would over-estimate all the C₃H₈ measurements without
480 degrading the strong correlation with C₂H₆, but seems unlikely.

481 3.3 Case Study: Ground-based measurements from JPL

482 The Jet Propulsion Laboratory (34.2N; 118.17W; 0.35 km altitude) lies at the Northern edge of the Los Angeles
483 basin. When winds are from the North (rare in summer) air quality is good. When conditions are stagnant (common
484 in summer) pollutants accumulate and so air quality is poor. C₃H₈ measured at JPL exhibits very different behavior
485 to that at Ft. Sumner. It decreases over time, exhibits little correlation with C₂H₆, and positive correlation with CO.
486 Figure 12 illustrates these behaviors.

487 The left-hand panels of Fig. 12 shows XC₃H₈ time series measured from JPL, color coded by CO. The upper-left
488 panel shows a large decrease in C₃H₈ from 1–3 ppb in 1990 to less than 1 ppb in 2019. This mirrors the decrease in
489 CO over JPL (not shown) over the same period. The lower-left panel shows a large seasonal component to the
490 C₃H₈, with a peak in late summer, when the air is most stagnant over JPL allowing pollutants to accumulate. The
491 highest C₃H₈ values appear red or orange (high CO), while the lowest appear blue (low CO), implying an
492 association with CO. This is confirmed in the upper-right panel which plots C₃H₈ directly against CO. The right-
493 hand panels are color-coded by year. The C₃H₈ correlation is mostly a result of both gases having decreased over the
494 30-year record. But even within each year, there still remains a positive correlation. This does not necessarily mean
495 that C₃H₈ and CO have the same source, but that their sources are spatially coincident.

Deleted: Of course, in cases of higher wind-speeds, or trajectories that partially circumvent the basin, the duration will be less than 8 hours and so the uptake of hydrocarbons will be smaller. ¶

Deleted: .

Deleted: always

Moved down [4]: One possibility is that the C₃H₈ coming from leaking wet NG is augmented by leaks of LPG, stripped from wet NG. This would further enhance the C₃H₈ (and C₄H₁₀) with little C₂H₆ increase.

Deleted: ¶

Formatted: Not Superscript/ Subscript

Deleted: /C₃H₈

Deleted: 5

Deleted: low

Deleted:

Deleted: m, but not all

Moved (insertion) [4]

Deleted: One

Deleted: leaking

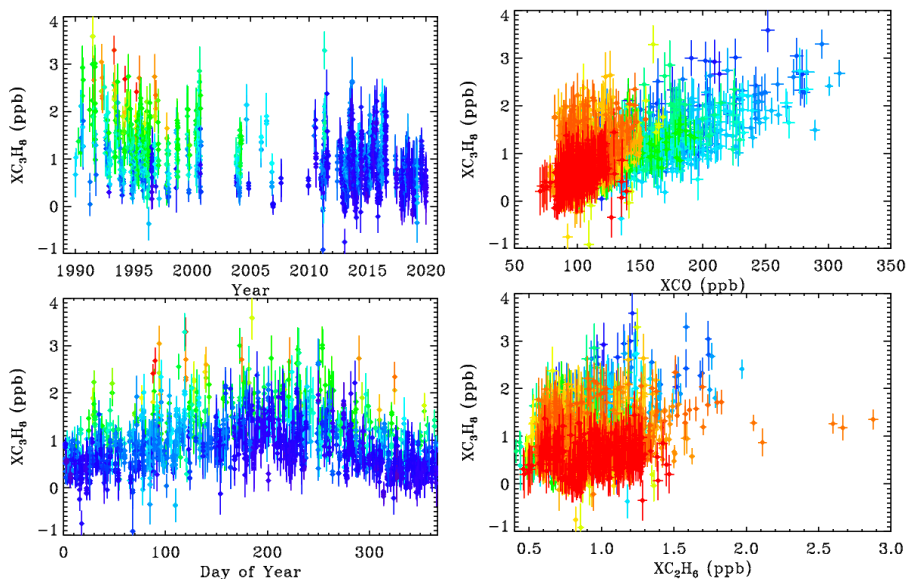
Deleted: ¶

¶

Deleted: 2

Deleted: 0

Deleted: 0



519

520 **Figure 12.** Column-average C_3H_8 above JPL. **Left Panels:** The time series color-coded by CO (red=250 ppb;
 521 green= 130 ppb; blue=100 ppb). **Right Panels:** The relationship between XC_3H_8 and CO and C_2H_6 color-coded by
 522 year (blue=1990; green=2005; red=2019).

523

524 The lower-right panel shows C_3H_8 plotted versus C_2H_6 . There is a weak correlation at JPL. The high XC_2H_6 values
 525 exceeding 2.0 ppb were measured in day 314 of 2015 when JPL was downwind of the Aliso Canyon NG leak.

526 Appendix C shows a HYSPLIT back-trajectory confirming this assertion. This spike can also be seen in Fig. 3.

527 There is no C_3H_8 enhancement associated with the C_2H_6 spike, since processed NG was leaking from an

528 underground storage facility, the heavy hydrocarbons (e.g., C_3H_8 , C_4H_{10}) having already been stripped out. A 2%
 529 increase in column-averaged CH_4 was also noted in the plume of the Aliso Canyon leak, as shown in Appendix C.

530 California accounts for less than 1% of total U.S. natural gas production and this has declined over the past three
 531 decades (<https://www.eia.gov/state/analysis.php?sid=CA>). Although there is natural gas extraction in the LA basin,
 532 this is a small source compared with the Permian basin. The local natural gas is only 3% C_2H_6 and 0.3% C_3H_8 ,
 533 (<https://www.socalgas.com/stay-safe/pipeline-and-storage-safety/playa-del-rey-storage-operations>) and so cannot
 534 account for the approximately equal amounts of these gases measured at JPL by the MkIV. We speculate that the
 535 C_3H_8 measured at JPL comes mainly from LPG (e.g., used in "clean" commercial vehicles, BBQ grills, external
 536 heaters, etc.). We can certainly rule out the possibility that the C_3H_8 measured at JPL is the result of wild fires, since
 537 these have increased in recent years whereas the C_3H_8 has decreased.

Deleted: 0

539 **3.4 Comparison with In Situ Measurements**

540 **First it should be pointed out that** the column-average mole fractions that are derived from the column measurements
541 will under-estimate the gas amount in the PBL for gases like C₂H₆ and C₃H₈ that reside mainly in the PBL. For
542 example, if C₃H₈ resides entirely between 1000 and 800 mbar, with none in the free troposphere or stratosphere,
543 then the column-average values will be 5 times smaller than the actual mole fractions in the PBL. So direct
544 comparisons of the remote and in situ mole fractions should be avoided. But their behavior as a function of year or
545 season, or gas-to-gas correlations, can still be meaningfully compared. This effect is in addition to the effect of their
546 averaging kernels being less than 1.0 at the surface, which was discussed earlier.

547 In situ C₃H₈ and C₂H₆ mole fractions from the Wendover, Utah (UTA) and Southern Great Plains, Oklahoma (SGP)
548 sites were downloaded from the NOAA Global Monitoring Laboratory website:
549 (<https://www.esrl.noaa.gov/gmd/dv/data/>). These sites are the closest to Ft. Sumner. These are surface flask
550 measurements covering the period 2006 to 2017. Figure 13 illustrates these data as a function of the year (left
551 panels), the day of the year (middle panels), and the C₃H₈-C₂H₆ relationship (right panels). The upper panels cover
552 the UTA site and the lower panels the SGP site. Note the factor 10 change in the y-scale: there is 10x more of these
553 gases at SGP than at UTA. Looking at the map in Fig. 11, this is clearly because SGP lies immediately downwind of
554 the Anadarko Basin oil and NG fields under the prevailing WSW winds. In contrast, the UTA site has no major up-
555 wind source.

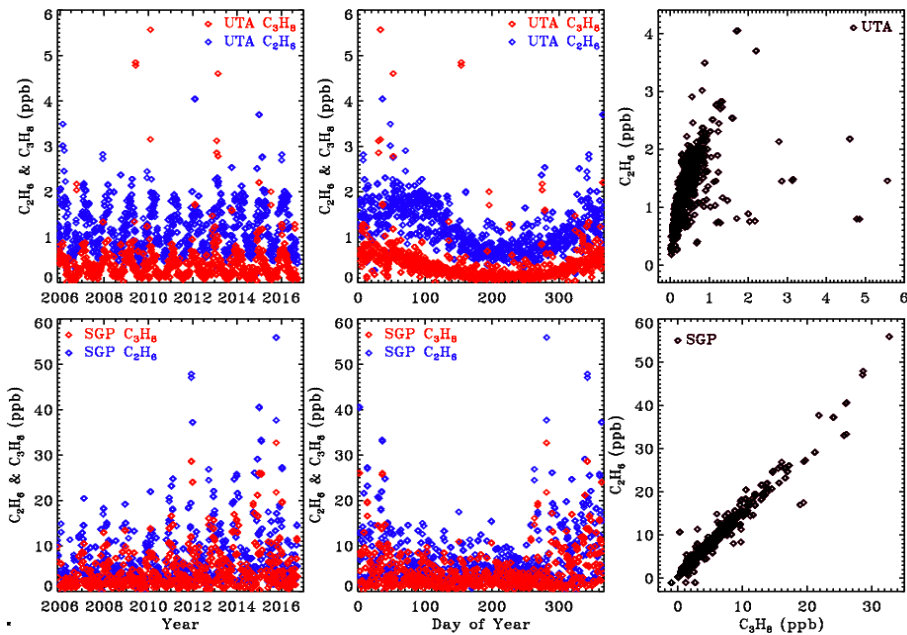
556 These in situ measurements confirm that C₃H₈ is highly variable with large enhancements being associated with oil
557 and NG production fields. At SGP the C₃H₈/C₂H₆ ratio is about 0.65. This is smaller than those measured by the
558 MkIV, but NG in the Permian basin is much wetter (richer in C₃H₈) than in the Anadarko basin.

Deleted: 3

Deleted: First a caveat:

Deleted: 1

Deleted: 9



563

564 **Figure 13.** In situ flask measurements of C_3H_8 (red) and C_2H_6 (blue) from the NOAA ESRL GMD dataset (Helmig
 565 et al., 2017). Top panels show results from the UTA site and lower panels from SGP. Note the factor 10 change in
 566 the y-scale between the two sites. Left panels plot data versus year to illustrate secular trends. Middle panels versus
 567 Day of year to more clearly see the seasonal cycle. Right panels plot C_3H_8 versus C_2H_6 .

568

569 **3.5. Balloon Results**

570 We also attempted to retrieve C_3H_8 from MkIV balloon solar occultation spectra. It was not detected in any flight,
 571 despite a very good sensitivity of 0.05 ppb above 5 km. This confirms that the C_3H_8 detected in ground-based
 572 measurements, reaching column average mole fractions of up to 4 ppb, resides mostly in the PBL. The balloon
 573 launches are typically performed only under stable, quiescent, meteorological conditions with light surface winds.
 574 Such conditions preclude uplift of air from the PBL into the free troposphere, so that C_3H_8 stays confined to the
 575 PBL, which is opaque in limb paths due to aerosol, and so cannot be probed in occultation. This does not preclude
 576 C_3H_8 getting up into the free troposphere at other times or in other places.

577

578

Deleted: 1

Deleted: 4

581 **4. Summary and Conclusions**

582 We report measurements of atmospheric C₃H₈ by solar absorption spectrometry in the strong Q-branch region at
583 2957 cm⁻¹, using high resolution IR spectra from the JPL MkIV interferometer. To the best of our knowledge, these
584 are the first remote sensing measurements of atmospheric C₃H₈. The minimum detectable abundance is about 10¹⁶
585 molecules.cm⁻², which is roughly equivalent to a column average mole fraction of 0.5 ppb. This allows C₃H₈ to be
586 measured in locations where its abundance is enhanced by proximity to sources (e.g., large gas fields, mega-cities),
587 but not in clean locations (e.g. above the PBL or away from sources). We encourage such NDACC and TCCON
588 sites to examine their datasets for C₃H₈. Future improvements to the spectroscopy of the interfering gases, e.g. H₂O,
589 CH₄, C₂H₆, and other CH-containing gases currently missing might even provide for the detection of C₃H₈ from
590 clean sites at background levels, allowing it to become a routine product of the NDACC and TCCON networks.

- Formatted: Subscript
- Formatted: Subscript
- Deleted: e
- Deleted: a

591 A case study of ground-based MkIV measurements from Ft. Sumner, New Mexico, shows increasing C₃H₈ and C₂H₆
592 amounts in the past decade on days when back-trajectories came from SE New Mexico and West Texas, where the
593 Permian Basin oil and gas field is located. A case study of C₃H₈ measured at JPL shows a long-term decrease since
594 1990 by more than a factor 2. It also shows a strong correlation with CO, a tracer of urban pollution. There is no
595 significant correlation between C₃H₈ and C₂H₆ at JPL.

596 The MKIV measurements in the case studies are not particularly useful for determining the long-term global trends
597 in C₃H₈ or C₂H₆, due to their close proximity to strong sources. In the case of the Ft. Sumner the source is the
598 Permian Basin. In the case of JPL the source is the Los Angeles urban area with a population of ~15M. These
599 sources cause large meteorology-driven fluctuations that mask the longer-term trends.

600 From balloon measurements in solar occultation, propane was analyzed using the same window as for the ground-
601 based measurements. It was not detected at any altitude in any of our 25 flights, despite a 0.05 ppb detection limit.
602 This is presumably because under the stable atmospheric conditions that allow balloon launches, C₃H₈ stays
603 confined to the PBL, which is opaque in the limb viewing geometry and so cannot be probed.

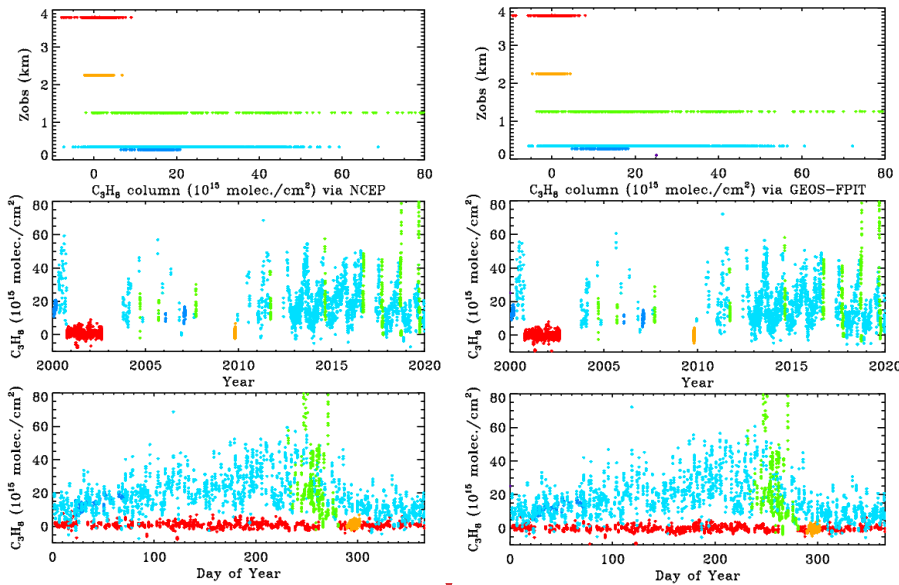
604 **Appendix A: Correlations between retrieved parameters**

605 We compute Pearson Correlation Coefficients (PCC) from the a posteriori covariance matrix for each of the 5000
606 spectral fits. The figures on the upper-left show the PCC between retrieved C₃H₈ and C₂H₆. Points are plotted versus
607 year with the same site-altitude-dependent coloring as in the other figures. The PCC between C₃H₈ and C₂H₆
608 averages about -0.7, which means that they are fairly strongly anti-correlated. This is due to their overlapping
609 absorption features at 2967.5 cm⁻¹. So as retrieved C₂H₆ increases, retrieved C₃H₈ will decrease, and vice versa. The
610 PCCs are closer to zero for the high-altitude sites (red & orange), presumably due to the reduced pressure
611 broadening and H₂O causing the C₂H₂ and C₂H₆ absorption features to become more distinct. This anti-correlation
612 could be reduced by use of a wider window to introduce additional C₂H₆ features that don't correlate with C₃H₈, but
613 this would also encompass large residuals without adding any C₃H₈ information.

- Formatted: Font: Times New Roman, Not Italic, Font color: Text 1
- Formatted: Line spacing: 1.5 lines
- Formatted: Font: Times New Roman, Not Italic, Font color: Text 1
- Formatted: Subscript
- Formatted: Font: Times New Roman, Not Italic, Font color: Text 1
- Formatted: Font: Times New Roman, Not Italic, Font color: Text 1
- Deleted: overlap the
- Deleted: Q-branch

640 analyses, which forms the basis of the latest (GGG2020) TCCON analysis (Laughner et al., 2021). We would have
 641 done the entire analysis with the GEOS-FP-IT model, except that it only supports the post-2000 time period.

642 Figure B.1 compares the retrieved C_3H_8 columns from the two analysis methods: NCEP in the left panels and
 643 GEOS-FP-IT in the right-hand panels. The results look very similar.

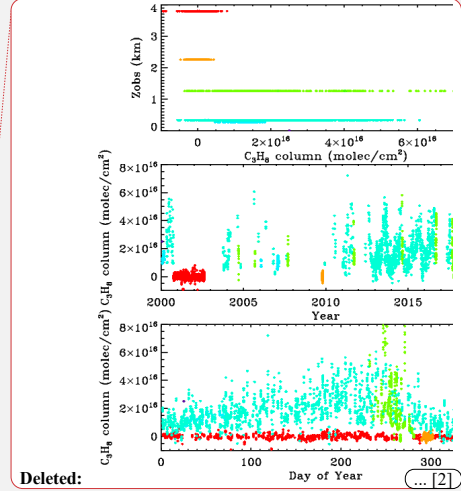


644
 645 **Figure B.1.** Retrieved vertical columns of C_3H_8 from 2000 to 2020 using two different atmospheric models. Left:
 646 NCEP a priori T/P/H₂O. Right: GEOS-FPIT a priori T/P/H₂O. Points are color-coded by site altitude, as in Fig. 3.

647 Figure B.2 examines more closely the C_3H_8 columns from the two analyses. In the upper panel the NCEP and
 648 GEOS-FPIT columns are plotted against each other. The gradient is 1.011 ± 0.003 with NCEP producing slightly
 649 larger columns. The Pearson correlation coefficient is +0.979. The column differences, shown in the lower panel,
 650 are mostly less than 5×10^{15} and are centered around zero at all column amounts. So the choice of models and priors
 651 makes surprisingly little difference to the retrieved C_3H_8 . This does not mean that the C_3H_8 is highly accurate. There
 652 are many things that are identical between the two analysis (e.g., spectroscopy, retrieval code, spectra) which could

Deleted: 0

Deleted: A



Deleted: ... [2]

Deleted: A

Deleted: Vertical columns of C_3H_8 retrieved using the

Deleted: Vertical columns of C_3H_8 retrieved using the

Deleted: -

Formatted: Indent: Left: 0", First line: 0"

Deleted: A

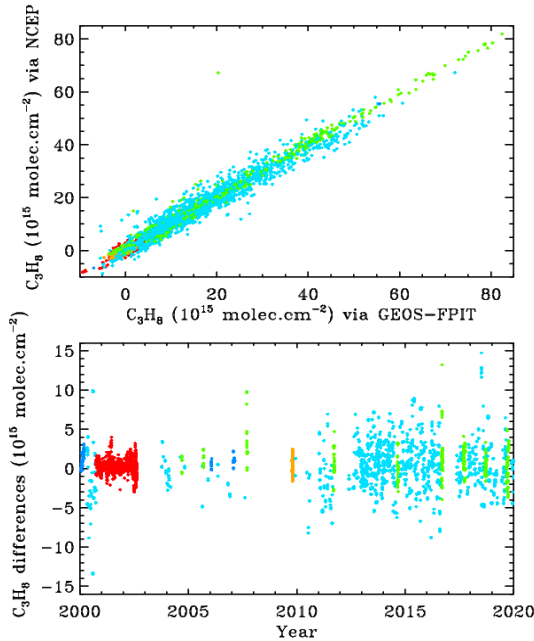
Deleted: 0.

Deleted: E⁺

Deleted: 6

Deleted:

667 nevertheless contribute large errors to the retrieved C₃H₈.

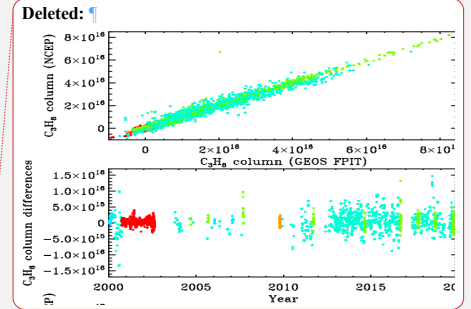


668

669 **Figure B.2.** Comparing the C₃H₈ columns retrieved from the 6-hourly NCEP and the 3-hourly GEOS-FPIT priors,
670 color-coded by site altitude. In the upper panel the columns are plotted against each other. In the lower panel their
671 difference is plotted.

672 **Appendix C: - Aliso Canyon Underground Storage Facility: Gas Leak in late 2015**

673 Aliso Canyon Underground Storage Facility is located 30 km NW of JPL. According to the Jan 4, 2016,
674 Los Angeles Times, NG leak began Oct 23, 2015 and peaked on Nov 28 at 60 Tons of CH₄ per hour. By Dec 22 leak
675 rate had decreased to 30 Tons per hour as the underground storage pressure dropped from the initial 2700 psi.



Deleted: A

Deleted: F

Deleted: Appendix B: C₃H₈ and C₂H₆ Averaging kernels
Figure B.1 shows all kernels for the 5000 measurements presented in this paper, color-coded by site altitude (red=3.8 km; orange=2.2 km; lime=1.2 km; cyan=0.35 km; blue < 0.2 km) as in the main body of the paper. The kernels increase with altitude but with <40% variation over the 0-30 km altitude range. Note that the kernels representing the 3.8 km site begin at P=0.7 atm. And the kernels representing the 2.2 km site begin at P=0.8 atm. [3]

Deleted: C



714

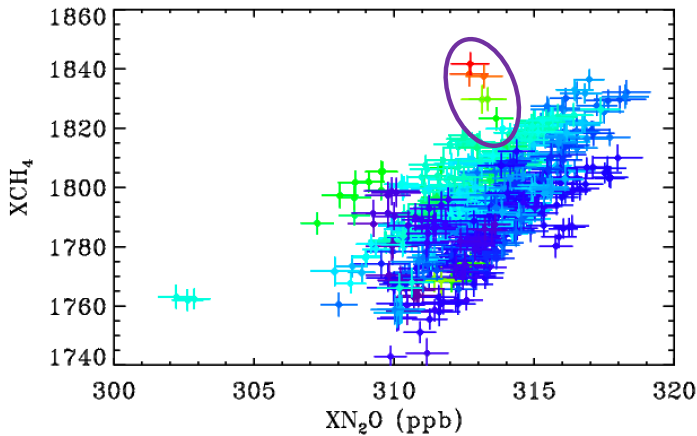
715 **Figure C.1.** HYSPLIT back-trajectories for Nov 10, 2015 (day 314) when the highest ever C_2H_6 was measured from
 716 JPL. Yellow oval (upper-left) indicates location of Aliso Canyon Underground Storage Facility. Green ball (lower-
 717 right) denotes JPL, at the convergence of trajectories arriving at 19, 20, & 21 UT. Trajectory calculation used the
 718 NAM 12 km resolution, hybrid sigma-pressure meteorology. © OpenStreetMap contributors 2020. Distributed under a
 719 Creative Commons BY-SA License.

720

721 Large C_2H_6 amounts (3x normal) were observed from JPL on Nov 10 (Day 314), but no enhancement of C_3H_8 .
 722 HYSPLIT back-trajectories for this day indicate that the air arriving at JPL at 1000m above ground was from the
 723 North-West and had passed over Aliso Canyon USF, confirming that the air over JPL was contaminated by the leak.

Deleted: C

Formatted: Line spacing: 1.5 lines



724

726 **Figure C.2.** Showing the relationship between CH₄ and N₂O at JPL in 2014–2017 color-coded by C₂H₆. Blue points
727 represent low C₂H₆ whereas red represents the highest C₂H₆. The encircled points represent Nov. 10, 2015, whose
728 back-trajectory is shown in [the](#) previous figure.

Deleted: C

729 Most of the variation in column CH₄ and N₂O is associated with the stratospheric circulation. Old airmasses from
730 high latitude are depleted in CH₄ and N₂O. To remove these effects, and be able to more clearly see changes driven
731 by the troposphere, XCH₄ is plotted versus XN₂O which is similarly affected by stratospheric circulation, but not by
732 tropospheric emissions. This creates a correlation with the lower-left points representing high-latitude stratospheric
733 airmasses and the upper right low-latitude airmasses.

734 The encircled points on Fig. C.2 were measured on Nov 10, 2015, when JPL was downwind of the Aliso Canyon
735 USF leak. The indicate XCH₄ enhancements of over 2%, which probably represent a 10+% enhancement in the
736 PBL with no enhancement above. There is also a general tendency for higher CH₄ values when C₂H₆ is elevated on
737 other days too, as seen from the dark blue points (low C₂H₆) being predominantly in the lower right of the figure and
738 the greener points (higher C₂H₆) being located toward the upper left.

Deleted: C

739

740 Code Availability

741 The GFIT code used for the analysis of MkIV spectra is identical to that used by the TCCON project. It is publicly
742 available under license from the California Institute of Technology for non-commercial use. It can be cloned from:

743 hg clone <https://parkfalls.gps.caltech.edu/tcon/stable/hg/ggg-stable/>
744 after signing the license agreement and being issued a password.

745

746 Data Availability

747 The ground-based MkIV data used in this paper can be downloaded from two sites:

748 <https://mark4sun.jpl.nasa.gov/ground.html>

749 <ftp://ftp.epc.ncep.noaa.gov/ndacc/station/barcroft/ames/ftir/>

Deleted: K

750 Authors Contributions

751 Toon, Sung, Blavier for data acquisition. Toon and Yu for data interpretation.

752 Competing Interests

753 No competing interests.

754 Acknowledgements

755 The authors gratefully acknowledge the NOAA Air Resources Laboratory (ARL) for the provision of the HYSPLIT
756 transport and dispersion model and/or READY website (<https://www.ready.noaa.gov>) used in this publication. [We](#)

760 [thank NCEP and GEOS FPIT for their atmospheric analyses.](#) We also acknowledge the NOAA ESRL GMD for
761 distributing in situ data of C₃H₈ and C₂H₆. We thank NASAs Upper Atmosphere Composition Observation (UACO)
762 program for funding support.

763 References

764 Angelbratt, J. et al. Carbon monoxide (CO) and ethane (C₂H₆) trends from ground-based solar FTIR measurements
765 at six European stations, comparison and sensitivity analysis with the EMEP model. *Atmos. Chem. Phys.* **11**,
766 9253–9269 (2011)

767 Conley, S., G. Franco, I. Faloon, D. R. Blake, J. Peischl, T. B. Ryerson, Methane emissions from the 2015 Aliso
768 Canyon blowout in Los Angeles. *Science* (2016), 351, (6279), 1317–1320

769 Dalsøren, S.B., Myhre, G., Hodnebrog, Ø. et al. Discrepancy between simulated and observed ethane and propane
770 levels explained by underestimated fossil emissions, *Nature Geoscience*, **11**, 178–184 (2018).

771 <https://doi.org/10.1038/s41561-018-0073-0>

772 Franco, B. et al. Retrieval of ethane from ground-based FTIR solar spectra using improved spectroscopy: recent
773 burden increase above Jungfraujoch. *J. Quant. Spec. Radiat. Trans.* **160**, 36–49 (2015).

774 Franco, B. et al. Evaluating ethane and methane emissions associated with the development of oil and natural gas
775 extraction in North America. *Environ. Res. Lett.* **11**, 044010 (2016).

776 [Harrison, J.J., Allen, N.D.C., and Bernath, P.F., 2010a, Infrared absorption cross sections for ethane \(C₂H₆\) in the 3](#)
777 [μm region, *Journal of Quantitative Spectroscopy and Radiative Transfer*, **111**, 357–363,](#)

778 [DOI: 10.1016/j.jqsrt.2009.09.010](#)

779 [Harrison, J.J. and Bernath, P.F., 2010b, Infrared absorption cross sections for propane \(C₃H₈\) in the 3 μm](#)
780 [region, *Journal of Quantitative Spectroscopy and Radiative Transfer*, **111**, 1282–1288,](#)

781 [DOI: 10.1016/j.jqsrt.2009.11.027](#)

782 [Helmig, D., Rossabi, S., Hueber, J. et al. Reversal of global atmospheric ethane and propane trends largely due to](#)
783 [US oil and natural gas production. *Nature Geosciences*, **9**, 490–495 \(2016\). <https://doi.org/10.1038/ngeo2721>](#)

784 [Helmig, D. et al. Climatology and atmospheric chemistry of the non-methane hydrocarbons ethane and propane over](#)
785 [the North Atlantic. *Elementa* **3** \(2015\).](#)

786 [Helmig D., Hueber J., Tans P. \(2017\), Non-Methane Hydrocarbons from the NOAA ESRL Surface Network, 2004–](#)
787 [2016.](#)

788 [Howard, Touché, Thomas W. Ferrara, Amy Townsend-Small \(2015\), Sensor transition failure in the high flow](#)
789 [sampler: Implications for methane emission inventories of natural gas infrastructure. *Journal of the Air & Waste*](#)
790 [Management Association](#), **65**:7, 856-862. DOI: [10.1080/10962247.2015.1025925](#).

791 Irion, F. W., Gunson, M. R., Toon, G. C., Chang, A. Y., Eldering, A., Mahieu, E., Manney, G. L., Michelsen, H. A.,
792 Moyer, E. J., Newchurch, M. J., Osterman, G. B., Rinsland, C. P., Salawitch, R. J., Sen, B., Yung, Y. L., and
793 Zander, R.: Atmospheric Trace Molecule Spectroscopy (ATMOS) Experiment Version 3 data retrievals, *Appl.*
794 *Opt.*, **41**, 6968–6979, 2002

Deleted: ¶

Formatted: Pattern: Clear (White)

Formatted: Font: (Default) Times New Roman, 10 pt

Formatted: Font: (Default) Times New Roman, 10 pt

Formatted: Font: (Default) Times New Roman, 10 pt

Formatted: Font: (Default) Times New Roman, 10 pt

Formatted: Font: (Default) Times New Roman, 10 pt

Formatted: Font color: Black

796 Rolph, G., Stein, A., and Stunder, B., (2017). Real-time Environmental Applications and Display sYstem: READY.
797 Environmental Modelling & Software, **95**, 210–228

798 Rosado-Reyes, C. M., and J. S. Francisco (2007), Atmospheric oxidation pathways of propane and its by-products:
799 Acetone, acetaldehyde, and propionaldehyde, J. Geophys. Res., 112, D14310, doi:10.1029/2006JD007566.

800 [Sharpe, Steven W. Johnson, Timothy J. Sams, Robert L. Chu, Pamela M. Rhoderick, George C. Johnson, Patricia](#)
801 [A., "Gas-Phase Databases for Quantitative Infrared Spectroscopy". *Applied Spectroscopy* **58**, 1452-1461, \(2004\)](#)

802 Stein, A.F., Draxler, R.R, Rolph, G.D., Stunder, B.J.B., Cohen, M.D., and Ngan, F., (2015). NOAA's HYSPLIT
803 atmospheric transport and dispersion modeling system, Bull. Amer. Meteor. Soc., **96**, 2059-2077

804 [Sung, K., G. Toon, A. W. Mantz, and M. A. H. Smith \(2013\), FTIR measurements of cold C₃H₈ cross sections at 7–](#)
805 [15 um for Titan atmosphere, *Icarus*, **226**, 1499–1513, doi:10.1016/j.icarus.2013.07.028](#)

806 Toon, G.C., The JPL MkIV Interferometer, *Opt. Photonics News*, **2**, 19–21, 1991

807 Toon, G. C., Blavier, J.-F., Sung, K., Rothman, L. S., and Gordon, I., HITRAN spectroscopy evaluation using solar
808 occultation FTIR spectra, J. Quant. Spectrosc. Ra., 182, 324–336, <https://doi.org/10.1016/j.jqsrt.2016.05.021>,
809 2016.

810 Toon, G. C., Blavier, J.-F. L., and Sung, K.: Atmospheric carbonyl sulfide (OCS) measured remotely by FTIR solar
811 absorption spectrometry, Atmos. Chem. Phys., 18, 1923–1944, <https://doi.org/10.5194/acp-18-1923-2018>,
812 2018a.

813 Toon, G. C., Blavier, J.-F. L., and Sung, K.: Measurements of atmospheric ethene by solar absorption FTIR
814 spectrometry, Atmos. Chem. Phys., 18, 5075–5088, <https://doi.org/10.5194/acp-18-5075-2018>, 2018b.

815 Wunch, D., Toon, G. C., Blavier, J.-F. L., Washenfelder, R. A., Notholt, J., Connor, B. J., Griffith, D. W. T.,
816 Sherlock, V., and Wennberg, P. O.: The total carbon column observing network, Philos. T. R. Soc. A, 369,
817 2087–2112, <https://doi.org/10.1098/rsta.2010.0240>, 2011.

818 Touché Howard, Thomas W. Ferrara & Amy Townsend-Small (2015) Sensor transition failure in the high flow
819 sampler: Implications for methane emission inventories of natural gas infrastructure, Journal of the Air & Waste
820 Management Association, 65:7, 856-862, DOI: 10.1080/10962247.2015.1025925

821 The NEED Project. (2017). Propane [pdf]. Retrieved from
822 <http://www.need.org/files/curriculum/infobook/propane.pdf>

823 Urbanski, Shawn P., Wei Min Hao and Stephen Baker, Chemical Composition of Wildland Fire Emissions, Chapter
824 4, Developments in Environmental Science, Volume 8, 79–107, A. Bytnerowicz, M. Arbaugh, A. Riebau, and
825 C. Andersen (Editors), ISSN: 1474-8177/DOI:10.1016/S1474-8177(08)00004-1

Formatted: Font: Times New Roman, 10 pt

Formatted: Font: 10 pt

Page 5: [1] Deleted Microsoft Office User 2/9/21 9:46:00 AM

▼.....
▲.....

Page 22: [2] Deleted Microsoft Office User 3/13/21 3:33:00 PM

▼.....
▲.....

Page 23: [3] Deleted Microsoft Office User 2/4/21 4:24:00 PM

▼.....